JSS Focus Issue on Gallium Oxide Based Materials and Devices

Switching Behavior and Forward Bias Degradation of 700V, 0.2A, β-Ga_2O_3 Vertical Geometry Rectifiers

Jiancheng Yang,[1] Chaker Fares,[1] Fan Ren,[1,*] Yen-Ting Chen,[2] Yu-Te Liao,[2] Chin-Wei Chang,[3] Jenshan Lin,[3] Marko Tadjer,[4] David J. Smith,[5] S. J. Pearton,[6,*,z] and Akito Kuramata[7]

[1] *Department of Chemical Engineering, University of Florida, Gainesville, Florida 32611, USA*
[2] *Department of Electrical and Computer Engineering, National Chiao Tung University, Hsinchu, Taiwan*
[3] *Department of Electrical and Computer Engineering, University of Florida, Gainesville, Florida 32611, USA*
[4] *US Naval Research Laboratory, Washington DC, USA*
[5] *Department of Physics, Arizona State University, Tempe, Arizona 85287, USA*
[6] *Department of Materials Science and Engineering, University of Florida, Gainesville, Florida 32611 USA*
[7] *Tamura Corporation and Novel Crystal Technology, Inc., Saitama 350-1328, Japan*

We report the switching recovery characteristics of large area (contact dimension 0.04 × 0.04 cm^2) vertical geometry β-Ga_2O_3 Schottky rectifiers, consisting of Si-doped epitaxial layers on conducting bulk substrates. Devices that were switched from forward current of 0.225 A to reverse off-state voltage of −700 V in an inductive load test circuit showed a recovery time (t_{rr}) of 82 ns, with a reverse recovery current (I_{rr}) of 38 mA and dI/dt of −2.28 A. μsec^{-1}. This shows the potential of Ga_2O_3 rectifiers for power switching applications, provided effective thermal management schemes can be implemented. Devices deliberately tested to failure under forward bias conditions exhibit delamination and cracking of the Ni/Au contact and underlying epitaxial Ga_2O_3 due to the low thermal conductivity of the Ga_2O_3. This failure mode is different to that under high reverse breakdown conditions, where pits formed by material failure under the high field generated at the edge of the rectifying contact occurs.

© The Author(s) 2019. Published by ECS. This is an open access article distributed under the terms of the Creative Commons Attribution 4.0 License (CC BY, http://creativecommons.org/licenses/by/4.0/), which permits unrestricted reuse of the work in any medium, provided the original work is properly cited. [DOI: 10.1149/2.0061907jss]

Manuscript submitted December 17, 2018; revised manuscript received January 21, 2019. Published January 30, 2019. *This paper is part of the JSS Focus Issue on Gallium Oxide Based Materials and Devices.*

Wide bandgap power devices based on SiC and GaN are gaining market share for use in power control and switching applications, lidar sensors for autonomous vehicles, multi-level converters, and motion control for robotics.[1–3] There is interest in extending the performance limits using other semiconductors that could potentially outperform SiC/GaN devices. β-Ga_2O_3 is emerging as a viable candidate for certain classes of power electronics with capabilities beyond existing technologies, due to its large bandgap (4.8eV) and the availability of large diameter (6 inch), relatively inexpensive substrates.[4–21] These applications include power conditioning systems, including pulsed power for avionics and electric ships, solid-state drivers for heavy electric motors and advanced power management and control electronics.[4,6,10]

The initial thrust on Ga_2O_3 electronics is targeted toward high power converters for both DC/DC and DC/AC applications. Ga_2O_3 Schottky diodes could supplement 600V Si or SiC rectifiers targeted at switch mode power converters.[4–12] High reverse breakdown voltages (up to 2300V) have been achieved in field-plated β-Ga_2O_3 vertical Schottky rectifiers fabricated on thick epitaxial layers on conducting substrates,[12,13] and lateral MOSFETs[21–26] have shown breakdown up to 1850V.[23] 1kV trench MOS-type Schottky barrier diodes and 1kV trench MOS-type normally off transistors have also been recently reported.[18,19] There has been less attention paid to the switching characteristics of these devices, with some reports of reverse recovery times of <30 ns for discrete rectifiers tested on a probe station.[12,13] A particular advantage of wide bandgap switching devices is that they should have lower on-resistances at a given bias and higher switching efficiency than Si.[1–4] Circuit simulations of Ga_2O_3 MOSFETs in a three phase modular multilevel converter showed lower conduction loss but higher switching loss than commercial SiC MOSFETs under the same conditions.[27,28] Measurements are needed of Ga_2O_3 device switching performance in inductive load test circuits to gain more understanding of the potential of this technology.

*Electrochemical Society Fellow.
zE-mail: spear@mse.ufl.edu

In this paper, we report the reverse recovery times and reverse recovery currents of Ga_2O_3 field-plated rectifiers switched from forward current of 0.225 A to reverse off-state voltage of −700 V. We find that under extreme forward bias conditions, where we deliberately induce failure, the devices exhibit delamination and cracking of the Schottky contact and underlying Ga_2O_3, indicating that thermal management is a key area for future advancement of these devices.

Experimental

The rectifiers were fabricated on 8 μm thick layers of Si-doped n-type Ga_2O_3 (n-type carrier concentration of 6.12 × 10^{15} cm^{-3} obtained from capacitance-voltage measurements) grown by Halide Vapor Epitaxy (HVPE) on β-phase Sn-doped Ga_2O_3 single crystal wafers with (001) surface orientation. These bulk wafers were grown by the edge-defined film-fed method with a carrier concentration of 3.6 × 10^{18} cm^{-3}. The X-ray diffraction full-width-half-maximum is <350 arc.sec for these substrates. High resolution cross-section Transmission Electron Microscopy (TEM) images show an absence of visible defects, as shown in Figure 1, indicating the high quality of the epitaxial layers and the underlying substrates.

The field-plated, edge terminated vertical rectifiers structures are shown in Figure 2 (top) and employed full area back-side Ti/Au ohmic contacts annealed under N_2 at 550°C for 30 sec.[12,13] The field-plate consisted of SiO_2/SiN_x dielectric layers (40/360 nm) deposited by plasma enhanced chemical vapor deposition. Dielectric windows were etched with 1:10 buffered oxide etch (BOE) and Ni/Au Schottky contacts (thickness 80 nm/420 nm) were deposited on the dielectric windows with 10μm overlap with the SiO_2/SiN_x dielectric layer. The devices we tested used a square contact area of 0.04 × 0.04 cm^2 (1.6 × 10^{-3} cm^2) -these are shown in the optical microscopy image at the bottom of Figure 2. Diode DC characteristics were carried out with an Agilent 4156C parameter analyzer for current and voltage level up to 100 mA and 100 V, respectively. For high voltage and current DC measurements, a Tektronix 370A curve tracer was used. A current

Downloaded on 2019-03-13 to IP 128.227.158.56 address. Redistribution subject to ECS terms of use (see ecsdl.org/site/terms_use) unless CC License in place (see abstract).

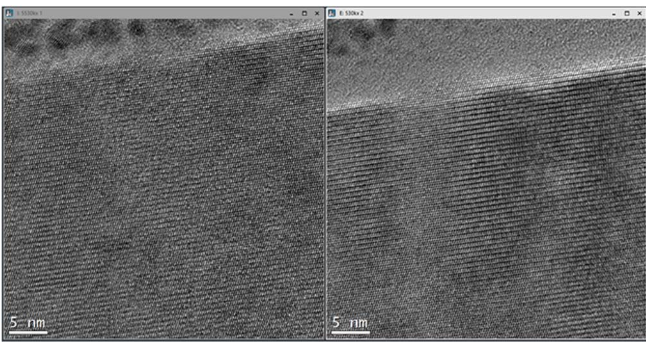

Figure 1. High resolution cross sectional TEM images from different regions in the Ga_2O_3 epi layer in the rectifier structure. The total epi thickness is 8μm, but we show expanded views of the near-surface to emphasize there are no visible defects from either growth or polishing.

probe along with a Micsig (DP10013) differential probe was used for the rectifier switching characteristic measurements.

Results and Discussion

Figure 3 shows the single-sweep forward and reverse current density (J-V) rectifier characteristics. The breakdown voltage (V_B) was 1900 V, with 1A of forward current at ~1V. The Schottky barrier height and ideality factor were 1.08 eV and 1.06, respectively. The on-state resistance, R_{ON}, was 0.24 Ω.cm^2, leading to a power figure of merit ($V_B{}^2$ /R_{ON}) of 15 MW.cm^2. These values are comparable to past reports for large area Ga_2O_3 rectifiers.[12,13,20]

A clamped inductive load test circuit was designed and fabricated for the switching measurements, whose operation is shown schematically in Figure 4. During the switching operation of the Ga_2O_3 rectifier, a double pulse was employed to drive the Si transistor, and the duration of the duty cycle used to adjust the Ga_2O_3 Schottky diode forward current.[29,30] The inductor is charged initially from the DC power supply when the transistor is turned on (accumulation mode). When it is turned off, the inductor releases charge through the forward-biased Ga_2O_3 rectifier (circulating mode). As the transistor is again turned on, the rectifier was switched from the on- to the off- state, where the charge was depleted. Finally, the current through the diode becomes zero.

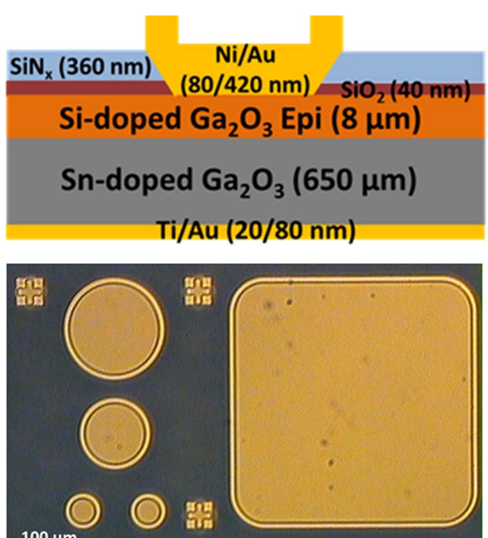

Figure 2. (top) Schematic of vertical geometry, field–plated rectifier structure and (bottom) optical microscope image of contact layout.

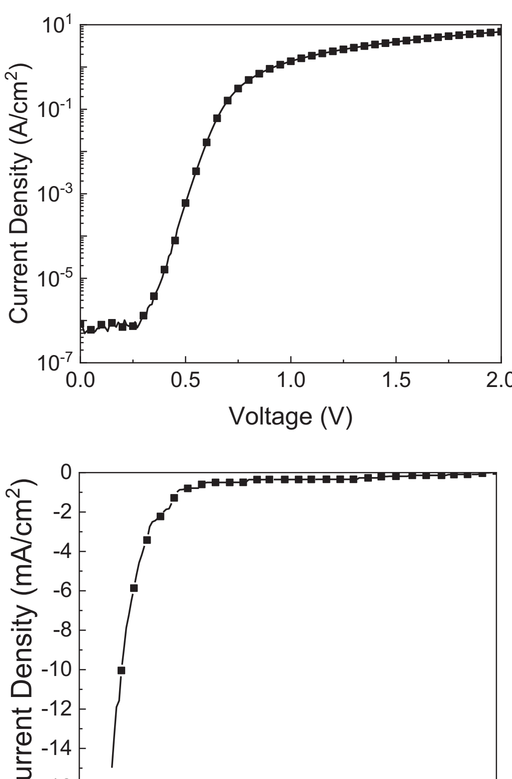

Figure 3. Forward (top) and reverse (bottom) current-density-voltage characteristics from rectifiers.

Figure 5 shows the switching performance and voltage waveform for the switching node of these rectifiers. The device was switched from 0.225 A forward current to a reverse voltage of −700 V. Our circuit boards and associated electronics are not rated for higher voltages, so we were not able to examine the full potential of the Ga_2O_3 rectifiers. The circuit was operated with a period of 50μsec, duty cycle 2%, MOSFET pulse was 10V and the power supply for the rectifier was 700V. The reverse recovery time, defined as the time that taken for rectifiers recover to the current level of 25% of the reverse recovery current, I_{rr}, was 82 ns with I_{rr} of 0.38 mA, and the dI/dt was −2.28 A/μsec. We have previously reported switching 1A of current to a reverse off-state voltage of −300V, with a recovery time of 64 ns and no significant temperature dependence of the recovery time up to 150°C,[29] while Takatsuka et al.[31] reported similar fast switching of Ga_2O_3 trench diodes. The switching recovery times are comparable to those reported for commercial SiC rectifiers.[32] While much remains

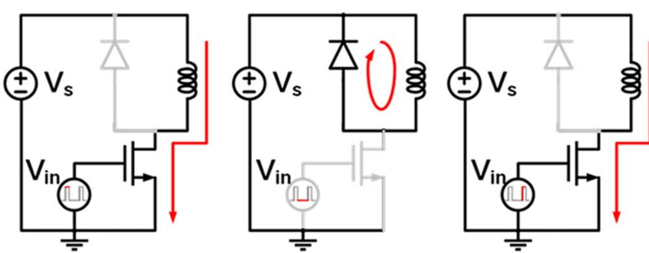

Figure 4. Schematic of operation of inductive load circuit for measuring dynamic switching characteristics of Ga_2O_3 rectifiers.

Downloaded on 2019-03-13 to IP 128.227.158.56 address. Redistribution subject to ECS terms of use (see ecsdl.org/site/terms_use) unless CC License in place (see abstract).

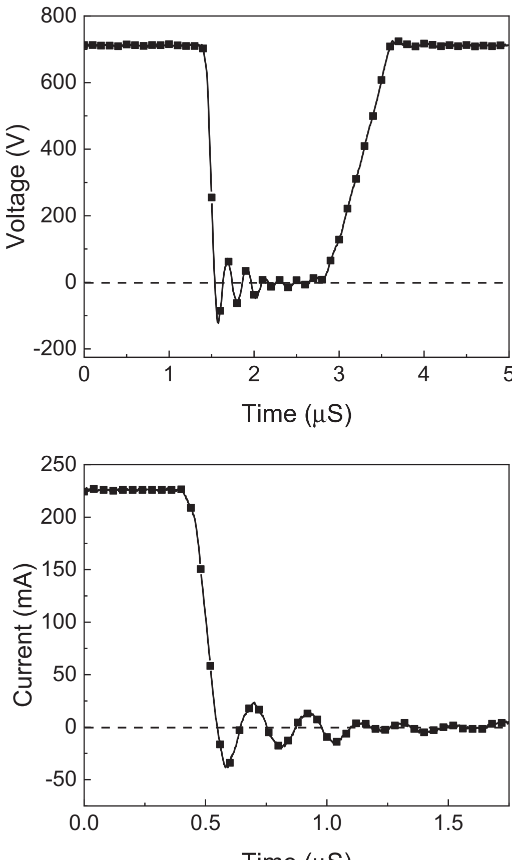

Figure 5. (top) Voltage waveform on the switching node during the diode switching measurement and (bottom) Rectifier switching from 0.225 A forward current to reverse off-state voltage of −700 V, showing τ_{rr} of 82 nsec.

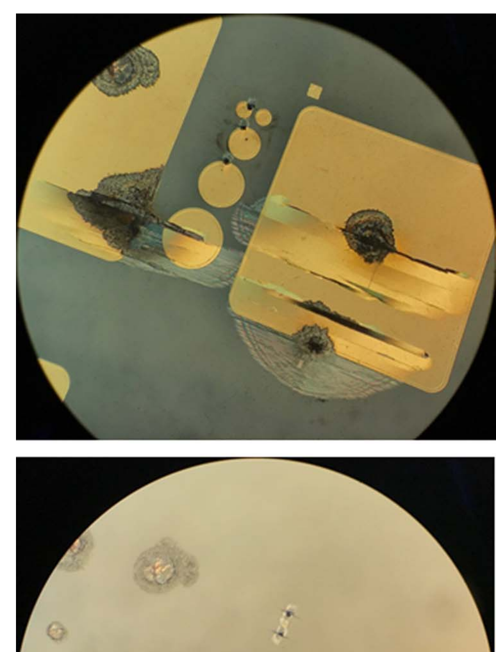

Figure 6. (top) Optical micrograph of Ni/Au contacted rectifier after forward bias testing to failure and (bottom) after removal of the Ni/Au contact.

to be optimized, including thermal management, plating technologies for current spreading and the field plate design, these results show the prospects for a role for β-Ga_2O_3 in power electronics.[6,9,10,30]

It is important to establish the failure mechanisms in these rectifiers under high current switching conditions. We have found that under very high reverse bias conditions, where continue increasing bias to deliberately induce degradation, these devices still fail by breakdown at the contact periphery.[33] This means the field plate design still needs additional optimization to avoid field crowding, which leads to avalanche multiplication of carriers. It is well established that the observed breakdown field in Ga_2O_3 devices is well below the theoretical limits. For example, 8 µm thick epi doped at $<10^{16}$ cm^{-3} has a theoretical breakdown of ~4.5 kV. If one deliberately tests the rectifiers to failure under reverse bias conditions, they breakdown at the rectifying contact periphery,[33] producing pits in the Ga_2O_3.

There has been less attention on the failure under forward bias conditions. Figure 6 (top) shows an optical microscope image of one of the large area contact devices after continued pulsed forward biasing under conditions deliberately designed to induce failure, displaying cracking and delamination of the Ni/Au contact. The bottom of the figure shows the same area after the Ni/Au was removed by etching in aqua regia and soaking in BOE. Some of the small pits from devices tested under reverse bias conditions are also visible in the center of the image. The devices tested under forward bias failure conditions show extended regions of cracks and delamination of the Ga_2O_3. Nanoindentation studies of single crystal Ga_2O_3 show hardness values of ~14.5 GPa obtained from the type of sample employed here.[34,35] In a study of the deformation of β-Ga_2O_3 under nanogrinding, the occurrence of crystallite defects in the ground subsurface was observed and the thermally-induced deformation that occurs during forward bias testing appear to also disrupt the crystallinity.[34,35] In a study of closely related single crystals of $Gd_3Ga_5O_{12}$, subsurface deformation was composed of a plastic flow zone, micro crack zone and median cracks.[36] The latter are caused by the severe slip of crystal planes subject to concentrated stress. It was found that lattice disorder is the precursor to plastic deformation under stress.[36] Wu et al.[35] found the deformation pattern of single crystal, (201) oriented β-Ga_2O_3 evolved with increased indentation load, beginning with stacking faults along the (200) lattice planes and twinning structures with the (201) plane as a twin boundary, followed by formation of dislocations on (101) lattice planes and finally, lattice bending and cracking. TEM imaging showed the (200) lattice planes were the preferred direction of cracking.[35] It should be noted that crack propagation and stacking faults lay on the same lattice planes, suggesting that the existence of stacking faults might help initiate cracking under mechanical loading.[35] The anisotropic nature of single crystal β-Ga_2O_3, means for example, that lattice planes of (200) and (002) are not symmetric equivalent,[4,8] thus different stress levels are required to introduce lattice deformation in different groups of lattice planes. This deformation sequence is unique to Ga_2O_3.[35,36]

To examine these regions more closely, we took images of these device pushed to very high pulsed current levels of >2A under forward bias. Figures 7 and 8 shows the cracks more clearly, while tilting the sample (Figure 9) reveals the associated delamination of the Ga_2O_3. The cracks are predominantly oriented along the [010] direction in our case. Preliminary thermal simulation results on the same device structure as used here show the maximum temperature rise was ~170K under these high power conditions.[37,38] The temperature rise and distribution in the rectifiers was simulated using self-consistent solution

Downloaded on 2019-03-13 to IP 128.227.158.56 address. Redistribution subject to ECS terms of use (see ecsdl.org/site/terms_use) unless CC License in place (see abstract).

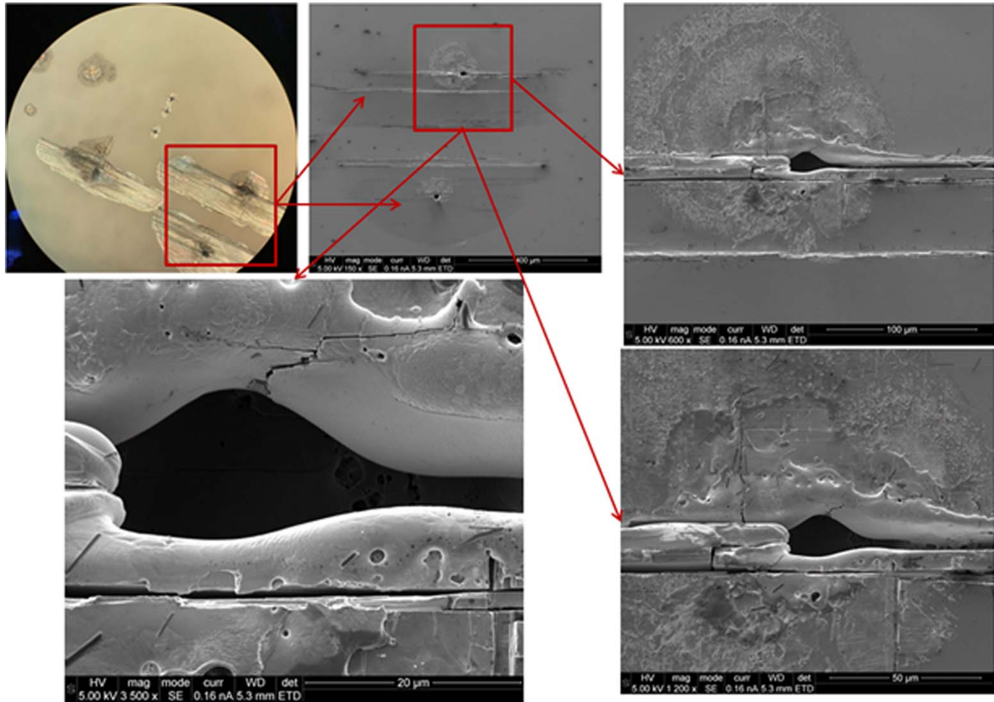

Figure 7. SEM images of the cracks and delaminated areas on the rectifier driven to forward bias failure.

of the partial differential equations governing the physics in the electrical and thermal domains with the Florida Object oriented device and process simulator (FLOODS) TCAD simulator. The actual temperature rise may be larger, since the Kapitza resistance or the Interfacial Thermal Resistance (ITR) was ignored in those first-order model although, there have been studies that show a temperature discontinuity at the interface due to the ITR.[39,40] Of course, the devices would be more susceptible to forward bias failure under DC conditions owing to the higher current and higher device temperatures under those conditions. There is an extensive literature on thermo-mechanical failure in forward-biased laser diodes.[41]

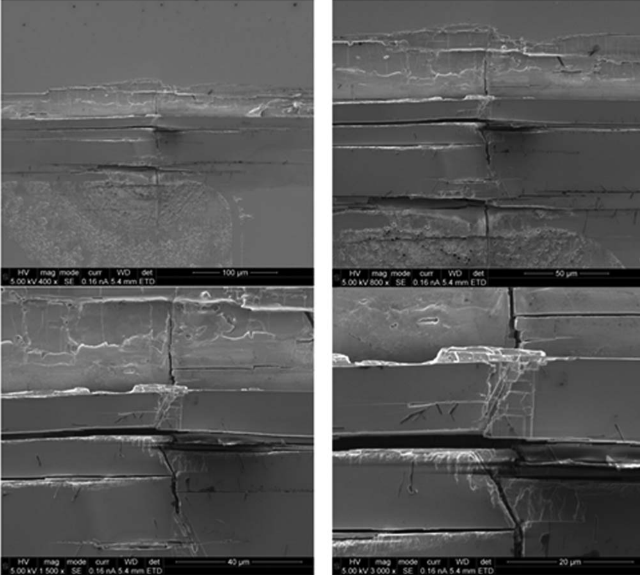

Figure 8. Close-up of cracks in the Ga_2O_3 in the failed devices.

The low thermal conductivity of Ga_2O_3 might be mitigated by integrating diamond as a high thermal conductivity heat spreader.[42–45] This has been successfully implemented for GaN RF devices, which may be operated at extreme, highly-localized power densities ($\sim 10^5$ W cm^{-2}).[44,46] Tadjer et al.[42] performed simulations of temperature rise in Ga_2O_3 epilayers on either a 200 μm thick Ga_2O_3 or a 50 μm thick Cu substrate as a function of epilayer thickness. Solving the heat equation for the two structures showed that significantly higher power density was required to reach 175°C by providing a high thermal conductivity path via Cu substrate. Thus, integration of Ga_2O_3 with diamond, which has nearly an order of magnitude higher thermal conductivity than Cu, would be an even more effective solution for high power Ga_2O_3 devices.[42,43] There have been initial experimental demonstrations of Ga_2O_3 on diamond which utilized a simple mechanical exfoliation process similar to that commonly employed for graphene.[43] Integrating top-side heat extraction will be an additional area for providing an effective thermal management strategy for Ga_2O_3.[47]

Conclusions

β-Ga_2O_3 vertical Schottky rectifiers with a forward current capability >1 A and 1900V reverse breakdown voltage were demonstrated with large area (1.6×10^{-3} cm^2). These devices were switched from 0.225 A to −700 V with t_{rr} of 82 ns, which shows the promise of high power Ga_2O_3 rectifiers for switching applications. Thermal management techniques will be important for these applications.

Acknowledgments

The project at UF was sponsored by the Department of the Defense, Defense Threat Reduction Agency, HDTRA1-17-1-011, monitored by Jacob Calkins. Research at NRL was partially supported by the Office of Naval Research, under contract N00014-15-1-2392. D.J.S. acknowledges the use of facilities in the John M. Cowley Center for High Resolution Electron Microscopy at Arizona State University.

Downloaded on 2019-03-13 to IP 128.227.158.56 address. Redistribution subject to ECS terms of use (see ecsdl.org/site/terms_use) unless CC License in place (see abstract).

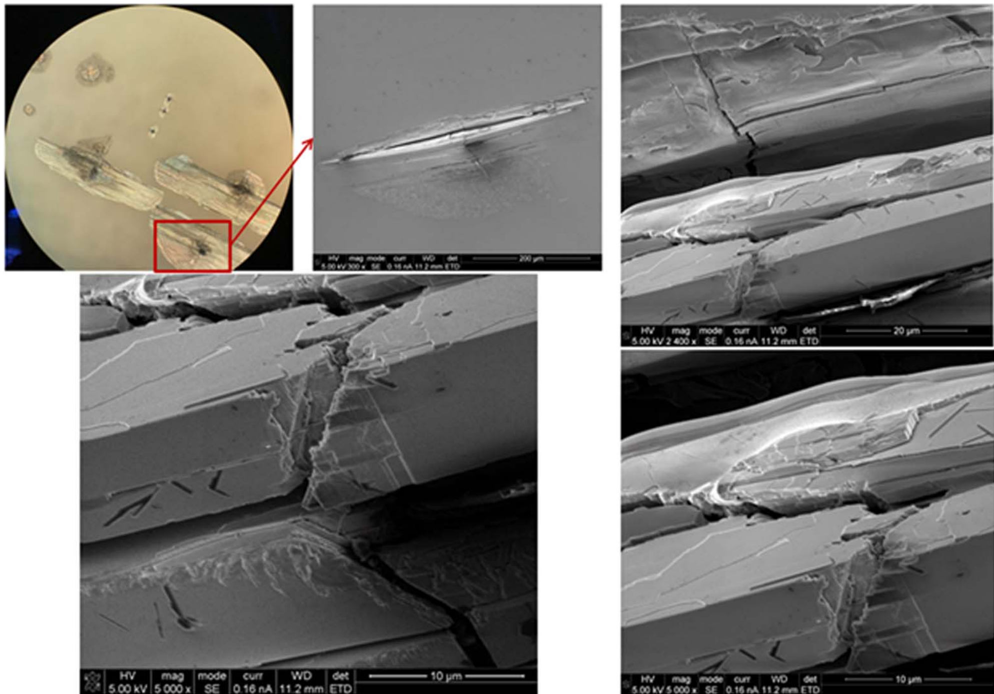

Figure 9. Tilted view of the delamination of the Ga_2O_3 after thermally-induced failure under forward bias conditions.

ORCID

Chaker Fares https://orcid.org/0000-0001-9596-2381
Fan Ren https://orcid.org/0000-0001-9234-019X
Jenshan Lin https://orcid.org/0000-0002-7439-9259
S. J. Pearton https://orcid.org/0000-0001-6498-1256

References

1. Alex Q. Huang, *Proc. IEEE*, **105**, 2019 (2017).
2. T. P. Chow, I. Omura, M. Higashiwaki, H. Kawarada, and V. Pala, *IEEE Trans Electron Dev*, **64**, 856 (2017).
3. Larry Spaziani and Lucal Lu, *Silicon, GaN and SiC: There's Room for All-Application space overview of device considerations, Proc. 30th Internat. Symp. Power Semicond. Devices and ICs*, May, 2018, Chicago, USA, 2018 Pages: 8 (IEEE, NY, 2018).
4. M. Higashiwaki, K. Sasaki, H. Murakami, Y. Kumagai, A. Koukitu, A. Kuramata, T. Masui, and S. Yamakoshi, *Semicond. Sci. Technol.*, **31**, 34001 (2016).
5. Marko J. Tadjer, Nadeemullah A. Mahadik, Jaime A. Freitas, Evan R. Glaser, Andrew D. Koehler, Lunet E. Luna, Boris N. Feigelson, Karl D. Hobart, Fritz J. Kub, and A. Kuramata, *Proc. SPIE 10532,Gallium Nitride Materials and Devices XIII*, 1053212 (23 February 2018).
6. M. Higashiwaki and G. H. Jessen, *Appl. Phys. Lett.*, **112**, 060401 (2018).
7. M. A. Mastro, A. Kuramata, Jacob Calkins, Jihyun Kim, Fan Ren, and S. J. Pearton, *ECS J. Solid State Sci. Technol*, **6**, P356 (2017).
8. S. J. Pearton, J. Yang, P. H. Cary, F. Ren, J. Kim, M. J. Tadjer, and M. A. Mastro, *Appl. Phys. Rev.*, **5**, 011301 (2018).
9. Xue Hui Wen, He QiMing, Jian Guang Zhong, Long Shi Bing, Pang Tao, and Liu Ming, *Nanoscale Research Letters*,**13**, 290 (2018).
10. S. J. Pearton, Fan Ren, Marko Tadjer, and Jihyun Kim, *J. Appl. Phys.*, **124**, 222901 (2018).
11. K. Konishi, K. Goto, H. Murakami, Y. Kumagai, A. Kuramata, S. Yamakoshi, and M. Higashiwaki, *Appl. Phys. Lett*, **10**, 103506 (2017).
12. J. Yang, F. Ren, M. Tadjer, S. J. Pearton, and A. Kuramata, *ECS J. Solid State Sci. Technol*, **7**, Q92 (2018).
13. J. C. Yang, Fan Ren, Marko J. Tadjer, and Akito Kuramata, *IEEE Trans. Electron Dev.*, **65**, 2790 (2018).
14. M. Oda, R. Tokuda, H. Kambara, T. Tanikawa, T. Sasaki, and T. Hitora, *Appl Phys Express*, **9**, 021101 (2016).
15. Z. Hu, K. Nomoto, W. Li, N. Tanen, K. Sasaki, A. Kuramata, T. Nakamura, D. Jena, and H. G. Xing, *IEEE Electr. Dev. Lett.*, **39**, 869 (2018).
16. Z. Hu, H. Zhou, K. Dang, Y. Cai, Z. Feng, Y. Gao, Q. Feng, J. Zhang, and Y. Hao, *IEEE J. Electron Devices Soc.*, **6**, 815 (2018).
17. Marko J. Tadjer, Andrew D. Koehler, Jaime A. Freitas Jr., James C. Gallagher, Matty C. Specht, Evan R. Glaser, Karl D. Hobart, Travis J. Anderson, Fritz J. Kub, Quang T. Thieu, Kohei Sasaki, Daiki Wakimoto, Ken Goto, Shinya Watanabe, and Akito Kuramata, *Appl. Phys. Lett.*, **113**, 192102 (2018).
18. Wenshen Li, Zongyang Hu, Kazuki Nomoto, Zexuan Zhang, Jui-Yuan Hsu, Quang Tu Thieu, Kohei Sasaki, Akito Kuramata, Debdeep Jena, and Huili Grace Xing, *Appl. Phys. Lett.*, **113**, 202101 (2018).
19. Zongyang Hu, Kazuki Nomoto, Wenshen Li, Zexuan Zhang, Nicholas Tanen, Quang Tu Thieu, Kohei Sasaki, Akito Kuramata, Tohru Nakamura, Debdeep Jena, and Huili Grace Xing, *Appl. Phys. Lett.*, **113**, 122103 (2018).
20. Jiancheng Yang, F. Ren, Marko Tadjer, S. J. Pearton, and A. Kuramata, *AIP Advances*, **8**, 055026 (2018).
21. H. Zhou, K. Maize, G. Qiu, A. Shakouri, and P. D. Ye, *Appl. Phys. Lett.*, **111**, 92102 (2017).
22. A. J. Green, K. D. Chabak, M. Baldini, N. Moser, S. Member, R. C. Fitch, G. Wagner, Z. Galazka, J. Mccandless, A. Crespo, K. Leedy, and G. H. Jessen, **38**, 790 (2017).
23. Ke Zeng, Abhishek Vaidya, and Uttam Singisetti, *IEEE Electron Dev Lett*. **39**, 1385 (2018).
24. K. D. Chabak, J. P. Mccandless, N. A. Moser, A. J. Green, K. Mahalingam, A. Crespo, N. Hendricks, B. M. Howe, S. E. Tetlak, K. Leedy, R. C. Fitch, D. Wakimoto, K. Sasaki, A. Kuramata, and G. H. Jessen, *IEEE Electron Dev Lett*. **39**, 67 (2018).
25. X. Yan, I. S. Esqueda, J. Ma, J. Tice, H. Wang, X. Yan, I. S. Esqueda, Y. Zhang, Chandan Joishi, Z. Xia, M. Brenner, S. Lodha, and S. Rajan, *Appl. Phys. Lett.*, **112**, 233503 (2018).
26. M. H. Wong, K. Sasaki, A. Kuramata, S. Yamakoshi, and M. Higashiwaki, *IEEE Electron Dev. Lett.*, **37**, 212 (2016).
27. Inhwan Lee, Avinash Kumar, Ke Zeng, Uttam Singisetti, and Xiu Yao, "Mixed-mode circuit simulation to characterize Ga_2O_3 MOSFETs in different device structures", 2017 *IEEE 5th Workshop on Wide Bandgap Power Devices and Applications (WiPDA)*, pp. 185 (2017).
28. I. Lee, K. Zeng, U. Singisetti, and X. Yao, "Modeling and power loss evaluation of ultra wide bandgap Ga_2O_3 devices for high power applications," in IEEE Energy Conversion Congress and Expo (ECCE), Cincinnati, OH, Oct. 1–5, 2017, Pages: 4377.
29. Jiancheng Yang, Fan Ren, Yen-Ting Chen, Yu-Te Liao, Chin-Wei Chang, Jenshan Lin, Marko J. Tadjer, S. J. Pearton, and Akito Kuramata, *IEEE J. Electron Dev. Soc.*, (in press, 2018).
30. Qiming He, Wenxiang Mu, Bo Fu, Zhitai Jia, Shibing Long, Zhaoan Yu, Zhihong Yao, Wei Wang, Hang Dong, Yuan Qin, Guangzhong Jian, Ying Zhang, Huiwen Xue, Hangbing Lv, Qi Liu, Minghua Tang, Xutang Tao, and Ming Liu, *IEEE Electron. Dev. Lett*, **39**, 556 (2018).
31. Akio Takatsuka, Kohei Sasaki, Daiki Wakimoto, Quang Tu Thieu, Yuki Koishikawa, Jun Arima, Jun Hirabayashi, Daisuke Inokuchi, Yoshiaki Fukumitsu, Akito Kuramata, and Shigenobu Yamakoshi, "Fast Recovery Performance of β-Ga_2O_3Trench MOS Schottky Barrier Diodes", *2018 76th Device Research Conference (DRC)*, pp. 1, June 2018.
32. T. Funaki, T. Kimoto, and T. Hikihara, *IEEE Trans. Power Electron.*, **23**, 2602 (2008).
33. Jiancheng Yang, Patrick Carey IV, Fan Ren, Yen-Ting Chen, Yu-Te Liao, Chin-Wei Chang, Jenshan Lin, Marko Tadjer, S. J. Pearton, David J. Smith, and Akito Kuramata, *Proc. SPIE Photonics West*, San Francisco, Feb 2019.

Downloaded on 2019-03-13 to IP 128.227.158.56 address. Redistribution subject to ECS terms of use (see ecsdl.org/site/terms_use) unless CC License in place (see abstract).

34. Shang Gao, Yueqin Wu, Renke Kang, and Han Huang, *Materials Science in Semiconductor Processing*, **79**, 165 (2018).
35. Y. Q. Wu, S. Gao, and H. Huang, *Materials Sci. Semiconductor Processing*, **71**, 321 (2017).
36. Chen Li, Feihu Zhang, Binbin Meng, Xiaoshuang Rao, and Yue Zhou, *Materials and Design*, **125**, 180 (2017).
37. B. Chatterjee, A. Jayawardena, E. Heller, D. W. Snyder, S. Dhar, and S. Choi, *Review of Scientific Instruments*, **89**, 114903 (2018).
38. Rohit Sharma, Erin Patrick, Mark E. Law, J. C. Yang, F. Ren, and S. J. Pearton, (sub to JSST).
39. G. Balasubramanian and I. K. Puri, *Appl. Phys. Lett.*, **99**, 13116 (2011).
40. T. Lu, J. Zhou, T. Nakayama, R. Yang, and B. Li, *Phys. Rev. B*, **93**, 85433 (2016).
41. see, for example, Osamu Ueda, in *Materials and Reliability Handbook for Semiconductor Optical and Electron Devices*, (Springer, NY, 2013).
42. Marko J. Tadjer, James C. Culbertson, Tatyana I. Feygelson, Virginia D. Wheeler, Jeffrey Woodward, Bradford B. Pate, Karl D. Hobart, Charles R. Eddy Jr., and Fritz J. Kub, *Towards Thermal Management of* β-Ga_2O_3 *by Integration with Diamond*, SPIE Photonics West, San Francisco, Feb 2019.
43. J. Noh, M. Si, H. Zhou, M. J. Tadjer, and P. D. Ye, *76th Dev. Res. Conf. Proc.*, 2018.
44. M. J. Tadjer, T. J. Anderson, J. C. Gallagher, P. E. Raad, P. Komarov, A. D. Koehler, K. D. Hobart, and F. J. Kub, in *76th Device Research Conference Proceedings* (IEEE, 2018).
45. P. Hindle, *Microw. J.*, **61**, 34 (2018).
46. T. J. Anderson, K. D. Hobart, M. J. Tadjer, A. D. Koehler, E. A. Imhoff, J. K. Hite, T. I. Feygelson, B. B. Pate, C. R. Eddy Jr., and F. J. Kub, *ECS J. Solid State Sci. Technol.*, **6**, Q3036 (2017).
47. Q. Hao, H. Zhao, Y. Xiao, and M. B. Kronenfeld, *Int. J. Heat Mass Transf.*, **116**, 496 (2018).

Downloaded on 2019-03-13 to IP 128.227.158.56 address. Redistribution subject to ECS terms of use (see ecsdl.org/site/terms_use) unless CC License in place (see abstract).